Electronic and Magnetic Properties of 2D/3D MnB: An Ab-initio & Monte Carlo Study

Izzet Parug Duru[1]
[1]Istanbul Gedik University, Department of Medical Imaging, Istanbul, Turkey

ABSTRACT

Defect-induced magnetic phases of 2D and 3D MnB were discussed. The exciting ferromagnetic behavior of MnB MBene is particularly tracked, including high-rated Mn defects via ab-initio calculations and Monte Carlo simulations. Ground state solution was achieved through GGA in PBESol scheme resulting in magnetic state and moments of Mn ions including the density of states around Fermi level. Magnetic susceptibility and magnetization behavior related to temperature was obtained through Monte Carlo simulations based on the Heisenberg model applying Metropolis criteria. The authors focused on controlling the Curie temperature considering the location of Mn defects. The coexistence of the various defect locations opened a realistic window to estimate Curie temperature consistent with experimental values. Exchange energies of 2D MnB different defect locations quite differ from each other. In addition, magnetic moments of the sheet material were found to be higher than 3D bulk MnB.

Keywords:
Monte Carlo method; Density functional theory; Defect formation; Ferrimagnetism; MnB sheet

INTRODUCTION

Graphene broadens the research area within magnetics, optics, thermo-electrics, and energy storage systems due to its wide and planar surface area. It has encouraged the production and discovery of other 2D materials. The researchers have been striving to introduce magnetism in these types of materials since they are not inherently magnetic. Fabrication of 2D materials possessing high Curie temperatures could foster the development of spin-based devices [1]. Besides, MXenes consisting of transition metal (TM) incorporated in Janus monolayers, are admirable to be used in further applications due to their electronic and magnetic behavior [2]. The van Hove singularities with huge electronic state densities near the Fermi level signify the instability in electronic interactions [3]. Thus, controlling magnetic behavior related to electronic properties can be possible by edge modification, applying external fields, and especially defect engineering [4]. Hence, this study focused on searching for defect-induced magnetic states in a 2D material and compared it to a 3D conjugate.

Defects can drastically alter the chemical environment of ions in crystal lattices, allowing for a wide range of material design possibilities. Theoretical calculations revealed itinerant magnetism in the existence of defects, which could explain the experimentally observed ferromagnetism with a high Curie temperature [5, 6]. Moreover, topological line defects driven in the material can be responsible for ferromagnetic stability and improving magnetic moments.[7]. Furthermore, dislocation and grain boundary in transition-metal constituted 2D MX_2 structures, may cause the transition from non-magnetic to ferromagnetic states [8]. Theoretical predictions of FM order and high carrier transport were experimentally verified by Zhang et al [9].

MBenes are also attractive additions to the 2D family which can be experimentally produced. Well, is it possible to obtain 2D MBenes? In short, 2D Metallic borides, (MnB, HfB, ZrB, etc.) provide remarkable stability. Moreover, 2D MnB MBenes create an enduring ferromagnetic (FM) phase. Extracting a 2D layer from a 3D crystal can be feasible due to the high thermal and mechanical stability of the material. Hexagonal intermetallic compound MnB_2 is antiferromagnetic (AFM) and the magnitude of the magnetic moments per manganese atom is 2.6μB [10]. However, Monte Carlo simulations showed that there is a strong local moment AFM possessing a high Néel temperature (TN) [11]. Khmelevskyi et al. showed that the ground state of MnB_2 is AFM ordered and the magnetic moment of Mn is approximately around 2μB [12]. Note that, Mn tetra-borides (MnB4) had a metallic ground state and possessed a

strong FM phase [13]. In the last decade, according to Gued-douh, Mn had a magnetic moment of 1.83μB [14]. In addition, TC of MnB was pretty close to 546.3K herewith a saturation magnetization of 155.5emu/g and a low coercive field [15]. The 2D MnB MBene sheet and its functionalized products exhibited a metallic FM behavior with the TC above room temperature (345K–600K) [16]. Thus, a new chapter had been opened presenting a low-cost and soft magnetic material. After functionalization with the –F and –OH groups, the TC was increased to 405K and 600K, respectively. Another study revealed that the MnB compound exhibited a large magnetocaloric effect at 570K [17]. According to first-principles calculations and Monte Carlo simulations to Mn2B2 sheet showed metallic FM behavior with 406K TC and 2.65μB magnetic moment satisfying excellent stability [18]. Hassan et al. realized that MnB2 is an AFM metallic material with Néel temperature, TN=810K [19] despite Klementz et al. revealed an FM [20] conduct.

Fabrication processes and theoretical approaches to magnetic and electronic properties of various 2D materials were presented by [21] in a wide spectrum. Even though well-known exchange mechanisms seem to be prominent to explain the nature of magnetism in magnetic materials, we presented a new insight to understand what is happening in the "magnetism cosmos" during stabilizing a magnetic phase in MnB 2D and 3D structure in the presence of Mn defects. Following ab-initio calculations, Monte Carlo simulations were performed considering Mn defects formed spontaneously-solely or simultaneously in the system. We focused on not only the defect-induced magnetic moments and TC values for bare and defected structures one by one but also track any joint contribution of considered cases. Section II was organized to introduce the structure, defect type, DFT, and Monte Carlo method used in calculations. Results were discussed in Section III and concluded in Section IV.

MATERIAL AND METHODS

Density functional theory (DFT) calculations are carried out via CASTEP [22] to obtain ground state solutions. Crystal structure of 3D MnB and 2D sheets are built on experimental lattice parameters as b=2.977Å, c=4.145Å [16] and illustrated in Figure 1 using VESTA [23]. It belongs to the Pnma space group as an orthorhombic crystal in the mmm point group. Cleaving the surface and creating a slab along "a" projection leads to a surface sheet of MnB. 4 different defect mode is proposed to not only figure out the most preferable one but also focus on the instantaneous extinction/formation frequency-dependent magnetic behavior. This work concentrated on inspecting the electronic structure induced by ferromagnetism. Furthermore, Monte Carlo methods, a versatile

and powerful tool, enable comprehension of the interesting relation through a randomized logic and a durable pipeline as simple as possible.

PBE-GGA is preferred to reveal the electronic structure of MnB including point defects created on different lattice sites. The optimization process using projector augmented-wave pseudo potentials for each defect scene was done accurately [24-26]. Plane-wave cutoff energy as 450eV and a Monkhorst-Pack 10x10x1 k-mesh are used. The minimization parameter of the total energy/atom convergence tolerance has been set to $1.0\times10^{-7}eV$. Tracing electronic structure makes it possible to discuss the metallic phase and magnetic state of the system. Authors have marked Mn ions introducing initial magnetic orders as AFM and FM causatively. The electronic minimization process allowed us to study both majority and minority spin channels through the density of states (DOS) and partial DOS (PDOS) of the system under the spin-polarized condition with Koelling-Harmon relativistic treatment. Exchange energies are calculated by directly subtracting the ground state energy of AFM order from FM order and considering spin moments obtained on each condition. Note that exchange couplings (J) vary due to the distinct distances between Mn ions and defect locations which also influence the spin magnetic moment of Mn. Markov Chain Monte Carlo (MCMC) simulation method based on the Metropolis algorithm [27] is chosen to provide simplicity and ergodicity. Heisenberg model rigorously represents the system involving a spin-spin interaction and the effect of the external magnetic field. TC can be determined from susceptibility measurements even one can infer it from the average magnetization versus temperature plot. It is crucial to obtain a high TC at least higher than room temperature for daily life usage. 60% of 1e9 MC steps stay sufficient for thermodynamic equilibrium and the rest is used to evaluate the expected values. The results section was divided into two parts: Ab-initio calculations and Monte Carlo simulations.

RESULTS AND DISCUSSION

Ab-Initio calculations: Density of states and ferrimagnetism

Geometry optimization and energy calculations are performed accurately for each ND and D, SMn, and VMn MnB structure via setting the initial magnetic interaction between Mn ions as AFM and FM, respectively. The resulting magnetic properties are found to be either AFM or FiM. Initially, AFM interacted Mn ions of ND structures end with AFM, and the rest end with FiM property. Table 1, presents detailed data obtained from the energy calculations considering 4 different locations (as illustrated in Figure 1) of Mn defects in the cell while exchan-
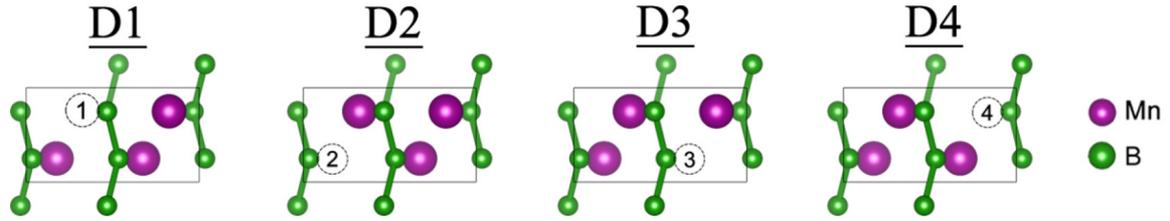
Figure 1. 4 different defect scenes are illustrated labeling point defects with a dashed circle. Defect locations are identical for the MnB sheet and bulk structures.

ging constant values of Mn pairs for ND and D, SMn, and VMn MnB are given in Table 2. We discovered that the most preferable defect locations are D2 of AFM VMn, D4 of AFM SMn, D3 of VMn FM, and D2 of FM SMn. However, spin densities of SMn are almost twice of VMn for all cases (ND and DX) when the initial magnetic order is FM. On the other hand, spin densities of VMn are quite lower than in the SMn case. Intriguingly, FM-ordered 3D MnB with ND possesses a notable exchange energy value in terms of eV between Mn pairs, JVMn-Mn, concerning ND SMn. On the other hand, defect formation caused a strong FM exchange coupling in D1 and D3 cases; herewith, Mn pairs exhibited an AFM coupling for the rest cases. The DOS for electrons with spin-up ($\rho_{Mn}^{\uparrow}$) and spin-down ($\rho_{Mn}^{\downarrow}$) Mn was obtained. Thus, the number of spin-up/spin-down electrons can be averaged with the aid of Equation 1. The magnetic moment of Mn (μMn)

can be calculated by subtracting the average number of spin-up electrons from the average number of spin-down electrons.

$$n^{Mn} = \int \rho^{Mn}(\varepsilon) d\varepsilon \qquad 1$$

Averaged magnetic moment of Mn of ND sheet MnB was found to be 2.54μB which is close to the result of Abdullahi et all. [18]. Defects led to the averaged magnetic moment of Mn decreasing on both structures as expected.

The average magnetic moments of the ND bulk (V) and sheet(S) structures were noted in Table 1. All Mn atoms that exist in ND structures had identical values while comma-separated moment values belong to the considered Mn ions that exist in DX (X=1,2,3,4) structures. Averaged magnetic moments of ND VMn and SMn were calculated as 1.87

Table 1. Final energy, magnetic property, spin density, and magnetic moment of MnB sheet and bulk structures including Mn defects. All samples possess metallic behavior.

Initial magnetic order	Defect position/No defect (ND)		Magnetic property	Integrated spin density (ℏ/2)	Integrated |spin density| (ℏ/2)	Magnetic Moment (μB)
AFM		ND	AFM	0	6.9345	-
	VMn	D1	FiM	2.0403	4.7091	-
		D2	FiM	2.0405	4.7162	-
		D3	FiM	-2.0401	4.7198	
		D4	FiM	2.0389	4.7185	-
	SMn	ND	AFM	0	11.8800	-
		D1	FiM	-0.5614	6.3897	-
		D2	FiM	-1.0007	5.9984	-
		D3	FiM	1.4552	8.0673	-
		D4	FiM	0.9395	7.3094	-
FM	VMn	ND	FiM	7.5668	8.5397	1.87 this paper, [ref 6] 2.71
		D1	FiM	3.5592	4.4441	1.68, 1.30, 0.68
		D2	FiM	3.5605	4.4459	1.30, 0.68, 1.68
		D3	FiM	3.5592	4.4441	1.68, 0.68, 1.30
		D4	FiM	3.5605	4.4459	0.68, 1.30, 1.68
	SMn	ND	FiM	10.0506	11.8310	2.54 this paper, [ref 7] 3.20, [ref 9] 2,65
		D1	FiM	6.9597	8.5364	2.88, 2.61, 1.66
		D2	FiM	6.9286	8.4880	2.59, 1.64, 2.90
		D3	FiM	7.0728	8.6151	2.95, 1.69, 2.61
		D4	FiM	6.9646	8.5387	1.67, 2.61, 2.89

and 2.54μB while defected MnB had moments of 1.22μB and 2.54μB for 3D (V) and 2D(S), respectively. Note that, B exhibited an antiparallel spin orientation with a negative moment. According to LSDA calculations of Park et all, Mn possesses a 1.795μB magnetic moment [28] and 1.91μB magnetic moment when GGA was used [29]. Defected structures obeyed spin symmetry according to the occupied sites with neighboring B atoms (Table 1). Unlike [16, 18], magnetic moments for ND structures were lower in this study. Our findings showed that both ND 3D and 2D MnB had a higher exchange coupling energy when compared to [16] results. Intriguingly, defect formation led to erratic discrepancies between exchange coupling values considered in this paper (D1, D2, D3, and D4 of SMn). In contrast, defects in the 3D MnB case resulted in similar values close to -18.8meV (Table 2) which is the main source of AFM. Note that, D1 and D3 defect orientations led AFM in 2D MnB as a part of an aforementioned strange situation. Various exchange mechanisms determining the magnetic state of a system were previously discussed [30-32]. Orbital hybridizations (s-p, p-d) related to the nature of the constituents seemed to explain the ferromagnetism in material properly. Note that, even though unpaired electrons and formerly mentioned mechanisms individually seem to determine the magnetic behavior, a joint act may lead to an inclusive picture. However, structural features essentially contribute to several physical properties on the nanoscale. Bond lengths are responsible for the electronic induced magnetic and optical properties of a material with also other intrinsic properties.

Total Density of states (TDOS) and Partial Density of States (PDOS) plots for all scenes are given in Figure 2 and Figure 3, respectively. So-called defect types can be regarded as a dramatic loss of the host Mn but not a trivial one. Metallic property of ND, Dx (x=1, 2, 3, 4) MnB 3D/2D was detected due to the Fermi level electrons providing intimate contact with valance and conduction bonds. ND 3D/2D AFM states preserved the up and down symmetry of DOS spin channels while the Fermi level electrons stood unbalanced at/around the Fermi level leading to the FM state as expected (Figure 2 and Figure 3).

The conduction band of AFM ND sheet and 3D cases had 2 similar peaks contributing to the density of electronic states at ~7eV and ~9eV, respectively. When defects were considered, DOS lines of AFM and FM 3D MnB were overlapped (Figure 5) in contrast to sheet MnB (Figure 4).

Highly defected 2D MnB gained an FM property even stronger than defected 3D MnB and ND sheet cases. Mn-d and B-p partial DOS plots of ND and D1 structures were given in Figure 6 and Figure 7, respectively. The hybridization between B-p and Mn-d orbitals is responsible for the magnetic behavior of the samples. One should deal with un-
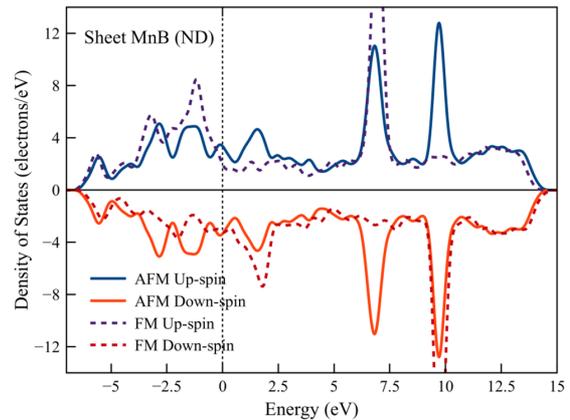
Figure 2. TDOS of ND FM and AFM MnB 2D.
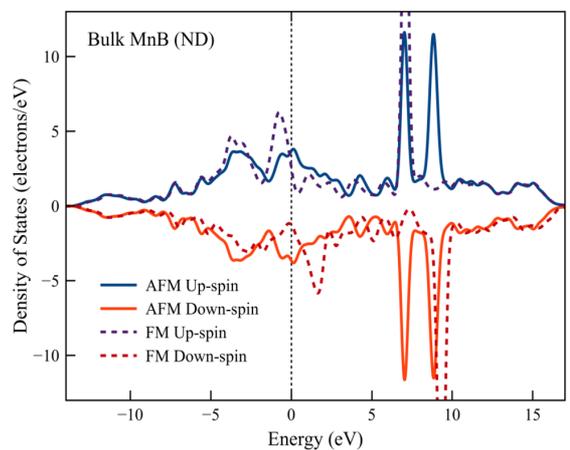
Figure 3. TDOS of ND FM and AFM 3D MnB.

paired electrons in d-orbitals of Mn considering the crystal field splitting effect of magnetism. The hybridization in the D1 sheet was stronger than in 3D D1. We focused on the range of -5eV and 5eV Mn-d contribution to electronic state at these energies is dominant but quite similar at other energies. Electrons at certain energies can be averaged around the Fermi level to calculate the magnetic moment and whistle about the feature of the magnetic behavior subtly.
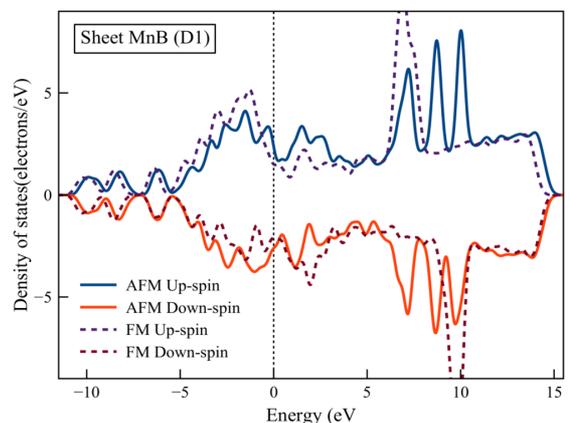
Figure 4. TDOS of D1 FM and AFM MnB sheet.
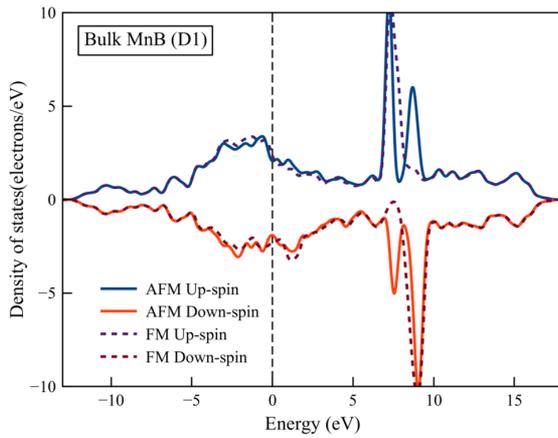
Figure 5. TDOS of D1 FM and AFM bulk MnB.
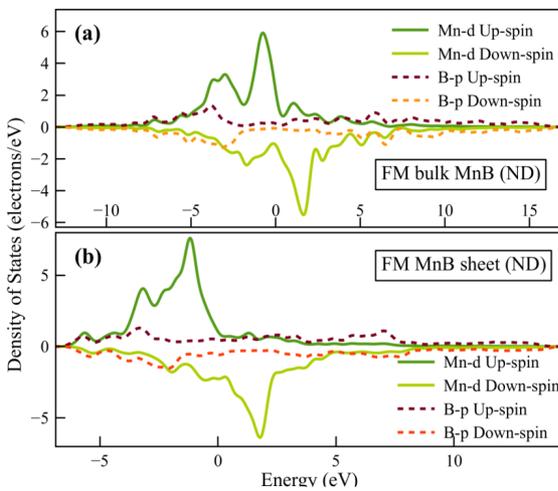
Figure 6. PDOS of ND FM bulk and sheet MnB. Greenish represents the Mn-d DOS while B-p contribution is visualized through reddish color.
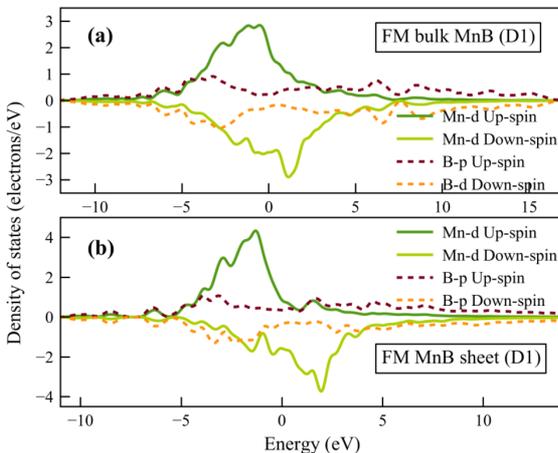
Figure 7. PDOS of D1 FM bulk and sheet MnB. Greenish represents the Mn-d DOS while B-p contribution is visualized through reddish color.

It is quite easier to bring out exchange coupling constants through the energy difference between AFM and FM states. Table 2, includes the exchange energies belonging to both ND and defected 3D and 2D structures revealing intri-

Table 2. Exchange energies between Mn ions for bare/defected volume and surface MnB crystal

Bulk(V)/ Sheet(S)	Defect(D)/No defect(ND)	JMn-Mn (meV)	[ref 7]
VMn	ND	165.41	
	D1	-18.76	
	D2	-18.80	
	D3	-18.71	
	D4	-18.78	
SMn	ND	8.55	3.1, 1.4 and -2.3
	D1	20.00	
	D2	-69.70	
	D3	103.93	

guing results which seem to be fair. In the 3D case, the negative sign calculated for considered defect locations emphasizes the AFM behavior. Moreover, the exchange energy did not vary in distinct defect positions.

The overall magnetic state does not depend on the location of defects. In contrast to the 3D case, this symmetry was broken in the 2D MnB case; thus, distinctive magnetic states were formed that were spotty with different signs: ND, D3, and D1 showed FM behavior while the rest is AFM. The absence of a defect (ND) led the MnB sheet to gain an FM behavior weaker than the ND 3D case. The exchange energies of Mn-Mn pairs belonging to 2D ND are quite higher than the findings of [16]. Moreover, D1 and D3 cases led to a dramatic increment in exchange energies when compared to [16] and also to ND.

Monte Carlo simulations: Susceptibility and Curie temperature

According to the Mermin-Wagner, FM and AFM can not exist in isotropic 2D systems because of the thermal fluctuations destructing long-range magnetic order [34]. Spin waves in 2D structures are relatively diluted when compared to 3D systems. This controls the size of the spin-wave gap with anisotropy. Consequently, long-range ordered magnetic 2D systems can be generated with the aid of anisotropy and the destructive effect of thermal agitations can be avoided. Additionally, lattice defects would interfere with the electronic states of the common orbitals of constituent atoms via overlapping state integrals. Considering crystal field, exchange mechanisms such as double and superexchanges rule the magnetic phase (FM, FiM, and PM) in local or the local moments of unpaired electrons interact directly. Note that, defect formation led to an increment in TC of sheets. Several approaches survived in the last decade to conceive the origin of ferromagnetism or ferrimagnetism focused on the orbital angles and/or unpaired electrons.

We are interested in the Curie temperature (TC) due to the importance of possessing a TC above room temperature to use in spintronic applications. Heisenberg model was used to represent the magnetic nature of the 3D/2D MnB in the case of ND and defects. Exchange coupling constants and magnetic moments obtained from first-principles calculations were used to drive Heisenberg Hamiltonian instead of XY and Ising model (Equation 2) on Monte Carlo (MC) simulations based on the Metropolis algorithm classically.

$$H = -\sum_{i,j} J_{ij}\vec{S}_{Mn}^{i}\vec{S}_{Mn}^{j} - \vec{B}\sum_{i}\vec{S}_{Mn}^{i} \qquad 2$$

J_{ij}, represents the exchange energy between Mn ions while $\vec{B}$ is the external magnetic field applied to the system. Only magnetic Mn atoms were considered to bring out phase transition temperature and magnetic susceptibility. 20x20x20 and 50x50 supercells were built for 3D and 2D MnB structures, respectively. The measurement process took 2×10^6 MC steps after the system achieved equilibrium. The applied procedure is just similar to what is done in previous works [32]. In contrast to MC logic, discussing the older findings in the literature, mean-field theory (MFT) had led to determine TC but led to a non-accurate result. According to Zhou Jiang, the fixed TC of MFT result is quite 345K [16]. We solely focused on 3D MnB in the ND case and MnB sheet for ND, D1, and, D3 cases due to the FiM states which were obtained from DFT calculations. Figure 8 and Figure 9 illustrated the MnB sheet and 3D structures, respectively, which were used in the determination of TC through Monte Carlo simulations.
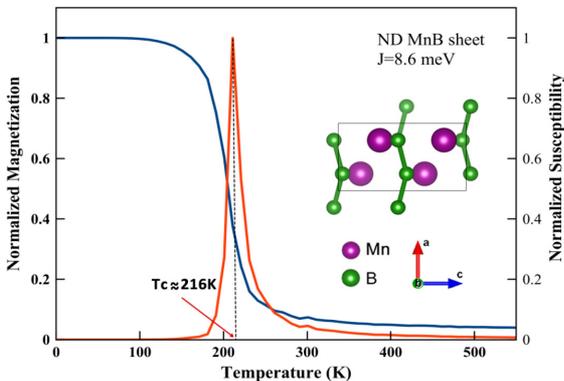
Figure 8. Normalized magnetization and susceptibility vs temperature of 50×50 ND MnB 2D sheet in which exchange coupling J=8.6meV. Purple and green spheres represent the Mn and B atoms, respectively.

Curie temperatures of ND and D1 MnB sheets were found to be close to 215K (Figure 8) and 551K (Figure 9), respectively while D3 MnB sheet and 3D ND cases retain relatively higher TC values greater than 1000K. D1 configuration (Figure 1) inspired a long-range FiM/FM order durable to the thermal agitations originated from higher temperatures
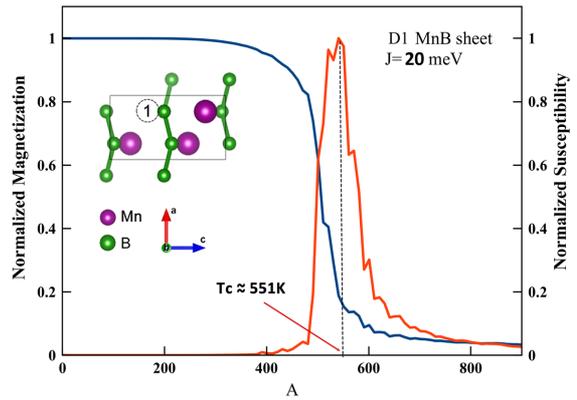
Figure 9. Normalized magnetization and susceptibility vs temperature of 50×50 D1 MnB 2D sheet in which exchange coupling J=20meV. Purple and green spheres represent the Mn and B atoms, respectively.

than ND MnB sheet (Figure 1) due to the relatively higher exchange energy as 20meV. According to the [16], 2D MnB sheets possessed TC values between 345K–600K while [18] found it as 406K with a magnetic moment of 2.65μB which is very close to 2.54μB of ND MnB sheet case. Mn Defect led some of the magnetic moments to increase (2.88 or 2.90μB) in lattice while when rest decreased to ~1.66μB. Latter is almost equal to the highest moment value of 3D defected MnB cases.

Magnetization vs. temperature and susceptibility vs. temperature plots were obtained performing Metropolis criteria and incorporating the contribution of ND, D1, D2, D3, and D4 simultaneously. It is to emphasize the joint distribution of distinct defect locations which can naturally occur in the same sample. The same procedure was applied for 3D MnB and the calculated TC was close to 422K (Figure 11) while 2D MnB joint structure possessed a higher value of 491K (Figure 10).
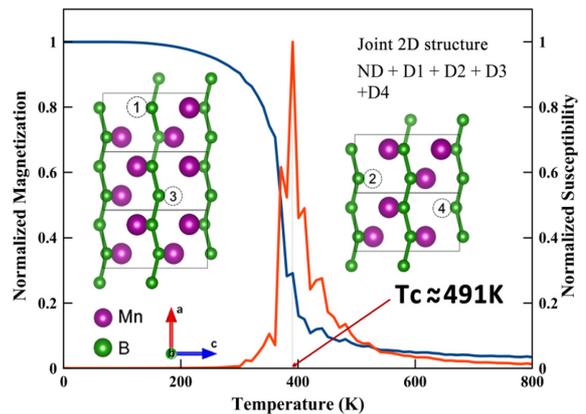
Figure 10. Normalized magnetization and susceptibility vs temperature of 50×50 MnB sheet in which exchange coupling of all samples are jointly adapted to the simulation. Purple and green spheres represent the Mn and B atoms, respectively.

TC of D1 was veritably close to 545K [20], 546.3K [15], and 570K [17] while joint 2D structure provides a relatively
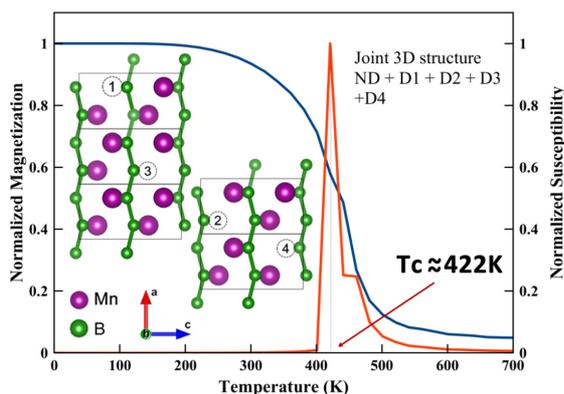
Figure 11. Normalized magnetization and susceptibility vs temperature of 20×20×20 MnB in which exchange coupling of all samples is adapted to the simulation. Purple and green spheres represent the Mn and B atoms, respectively.

lower value of 491K. However, ND 3D and D3 2D MnB overestimated Curie temperature pretending they were hard magnets. Hence, the joint structure provided a more realistic prediction of Curie temperatures when the abovementioned structures were considered.

The exchange mechanisms based on orbital interactions play a crucial role in the magnetic state of a system with distant dependency. Broken symmetry and joint contribution of ND, D1, D2, D3, and D4 in the 2D sheet were decisively determining the resulting FM, particularly in the existence of defects. In contrast, 3D structure substantially preserved the symmetry and defects leading to an interruption in all spatial directions. Note that, one can tune Curie temperature via setting the locations of Mn defects within the sheet.

CONCLUSION

Theoretical aspects take place to elaborate on the origin of magnetism in an atomic manner, especially, when it is difficult to experimentally produce those structures such as 2D materials and control large defects. In this study, defect formation in MnB sheets was related to the favored magnetic behavior and the effect of defect locations in the crystal that jointly exist. Each MnB 2D, 3D bare and defected structure showed the metallic ferrimagnetic property. Magnetic moments of Mn in sheets were stronger than 3D case. Besides, the difference between the majority and minority spins around the Fermi level emphasized the FM behavior. Curie temperature can be controlled by setting the locations of Mn defects within the sheet material. However, random Mn defects substantially correspond to a joint formation of a bare and defect-included structure that should be treated as containing Mn defects in distinct sites. A suitable Curie temperature was obtained from such a system as 551K which is consistent with the findings of previous studies given in the results section. In addition, broken symmetry and

joint contribution of ND, D1, D2, D3, and D4 in the 2D sheet were decisively determining the resulting FiM/FM, particularly in the existence of defects.

ACKNOWLEDGEMENT

CONFLICT OF INTEREST

The authors declare that they have no known competing financial interests or personal relationships that could have appeared to influence the work reported in this paper.

References

1. Swartz AG, Odenthal PM, Hao Y, Ruoff RS, Kawakami RK. Integration of the ferromagnetic insulator EuO onto graphene. ACS Nano 6 (2012) 10063–10069.

2. Gao, P.; Song, M.; Wang, X.; Liu, Q.; He, S.; Su, Y.; Qian, P. Theoretical Study on the Electronic Structure and Magnetic Properties Regulation of Janus Structure of M'MCO2 2D MXenes. Nanomaterials (12) 2022 556.

3. Van Hove L. The occurrence of singularities in the elastic frequency distribution of a crystal. Physical Review 89 (1953) 1189–1193.

4. Miao NH, Sun ZM, Computational design of two dimensional magnetic materials. Wiley Interdisciplinary Reviews. WIREs Computational Molecular Science. 5 (2021) e1545.

5. Yazyev OV, Helm L. Defect-induced magnetism in graphene. Physical Review B 75 (2007) 125408.

6. Wang Y, Huang Y, Song Y, Zhang X, Ma Y, Liang J, et al. Room-temperature ferromagnetism of graphene. Nano Letters 9 (2009) 220–224.

7. Kou L, Tang C, Guo W, Chen C. Tunable magnetism in strained graphene with topological line defect. ACS Nano 5 (2011) 1012–1017.

8. Zhang Z, Zou X, Crespi VH, Yakobson BI. Intrinsic magnetism of grain boundaries in two-dimensional metal dichalcogenides. ACS Nano 7 (2013) 10475–10481.

9. Zhang M, Wang X, Sun H, Wang N, He J, Wang N, Long Y, Huang C, Li Y. Induced ferromagnetic order of graphdiyne semiconductors by introducing a heteroatom. ACS Central Science 6 (2020) 950–958.

10. Legrand E, Neov S. Neutron diffraction study of MnB2. Solid State Communications 10 (1972) 883-885.

11. Khmelevskyi S, Mohn P. Magnetic ordering in MnB2: an ab initio study. Solid State Communications 113 (2000) 509-512.

12. Khmelevskyi S, Mohn P. Covalent magnetism, exchange interactions and anisotropy of the high temperature layered antiferromagnet MnB2. Journal of Physics: Condensed Matter 24 (2012) 016001.

13. Khmelevskyi S, Redinger J, Shick AB, Mohn P. One-dimensional magnetism of one-dimensional metallic chains in bulk MnB4. Condensed Matter 1-11 (2013)

14. Gueddouh A. The effects of magnetic moment collapse under high pressure on physical properties in mono-borides TMB (TM = Mn, Fe): a first-principles. Phase Transitions 9 (2017) 984-1000.

15. Ma S, Bao K, Tao Q, Zhu P, Ma T, Liu B, Liu Y, Cui T. Manganese

mono-boride, an inexpensive room temperature ferromagnetic hard material. Scientific Reports 7 (2017) 43759.

16. Jiang Z, Wang P, Jiang X*, Zhao J, MBene (MnB): a new type of 2D metallic ferromagnet with high Curie temperature. Nanoscale Horizons 3 (2018) 335.

17. Bocarsly JD, Levin EE, Humphrey SA, Faske T, Donner W, Wilson SD, Seshadri R. Magnetostructural coupling drives magnetocaloric behavior: The case of MnB versus FeB. Chemistry of Materials 31 (2019) 4873–4881.

18. Abdullahi YZ, Vatansever ZD, Aktürk E, Akıncı Ü, Aktürk OÜ. A tetragonal phase Mn2B2 sheet: a stable room temperature ferromagnet with sizable magnetic anisotropy. Physical Chemistry and Chemical Physics 22 (2020) 10893-10899.

19. Ahmoum H, Boughrara M, Su'ait MS, Li G, Rai DP, Kerouad M, Wang Q. Monte Carlo and Density functional theory investigation on the magnetic nature properties of MnB2. Applied Journal of Environmental Engineering Science 6 (2020) 429-435.

20. Klemenz S, Fries M, Dürrschnabel M, Skokov K, Kleebe HJ et al., Low-temperature synthesis of nanoscale ferromagnetic α'-MnB. Dalton Transactions 9 (2020) 131-135.

21. Jiang X, Liu Q, Xing J, Liu N, Guo Y, Liu Z, Zhao J. Recent progress on 2D magnets: Fundamental mechanism, structural design and modification. Applied Physics Review 8 (2021) 031305.

22. Clark SJ, Segall MD, Pickard CJ, Hasnip PJ, Probert MIJ, R Keith, CP Mike. First-principles methods using CASTEP. Zeitschrift fuer Kristallographie 220 (2005) 567-570.

23. Momma K, Izumi F. VESTA: a three-dimensional visualization system for electronic and structural analysis. Journal of Applied Crystallography 41 (2008) 653-658.

24. Blochl PE. Projector augmented-wave method. Physical Review B 50 (1994) 17953.

25. Kresse G, Furthmuller J. Efficiency of ab-initio total energy calculations for metals and semiconductors using a plane-wave basis set. Computational Materials Science 6 (1996) 15.

26. Kresse G, Joubert D. From ultrasoft pseudopotentials to the projector augmented-wave method. Physical Review B 59 (1999) 1758.

27. Metropolis N, Rosenbluth AW, Rosenbluth MN, Teller AH, Teller E. Journal of Chemical Physics 21 (1953) 1087.

28. Park J, Hong Y-K, Kim H-K, Lee W, Yeo C-D, Kim S-G, Jung M-H, Choi C-J, Mryasov ON. Electronic structures of MnB soft magnet. AIP Advances 6 (2016) 055911.

29. Simsek T, Ozcan S. Structural and Magnetic Properties of MnxB100−x Alloys. IEEE Transactions on magnetism 51 (2015) 2001903.

30. Duru IP, Ozugurlu E, Arda L. A first-principles study of magnetic properties of Zn0.94Mg0.01Mn0.05O. Materials Research Express 6 (2019) 126118.

31. Duru IP, Ozugurlu E, Arda L, A first-principles study of Mg/Ni induced magnetic properties of Zn0. 95− xMgxNi0. 05O. Journal of Magnetism and Magnetic Materials 504 (2020) 166653.

32. Duru IP, Ozugurlu E, Arda L. Size effect on magnetic properties of Zn0.95−xMgxNi0.05O nanoparticles by Monte Carlo simulation. Ceramics International 45 (2019) 5259-5265.

33. Mermin ND, Wagner H. Absence of ferromagnetism or antiferromagnetism in one- or two-dimensional isotropic Heisenberg models. Physical Review Letters 17 (1966) 1133–1136.